Advanced Steel Construction – Vol. 21 No. 5 (2025) 436–447
DOI:10.18057/IJASC.2025.21.5.6

EXPERIMENTAL RESEARCH ON MECHANICAL PERFORMANCE OF COLD-FORMED THIN-WALL FABRICATED RACK COLUMNS

Yan-Bo Qu [1], Gan Tang [1,*], Ling-Feng Yin [2] and Ren-Yi Shi [1]

[1] *Department of Civil and Airport Engineering, Nanjing University of Aeronautics and Astronautics, Nanjing, 211106, China*
[2] *School of Civil Engineering, Southeast University, SiPaiLou 2, Nanjing 210096, China*
** (Corresponding author: E-mail: tanggan@sina.com)*

ABSTRACT

The increasing prevalence of thin-wall fabricated rack has heightened demands on the load-bearing capabilities of structural components, particularly columns. Traditional cold-formed thin-wall single-limb columns are now often inadequate for safety standards, prompting the need for innovative column designs and reinforcement techniques. A prevalent reinforcement strategy involves transforming single-limb columns into double-limb configurations. This study employs experimental and theoretical analyses to evaluate the mechanical properties of both single-limb and double-limb columns, proposing reinforcement methods such as force transfer plates. The research includes: (1) designing load-bearing tests for both column types to determine load-displacement curves and ultimate capacities; (2) developing an enhanced finite element model to validate mechanical performance against experimental data; and (3) conducting a parametric study on factors influencing the mechanical behavior of double-limb columns, providing guidelines for their practical application.

ARTICLE HISTORY

Received: 4 August 2024
Revised: 16 January 2025
Accepted: 6 February 2025

KEYWORDS

Steel storage rack;
Cold-formed thin-walled;
Coupled composite column;
The simulation of the finite element model;
Parametric analysis

1. Introduction

In the past, the storage industry was dominated by ordinary warehouses, with a single structure and a simple function. With the rapid development of other upstream industries, the storage industry has also developed from the original single to the diversified, from a simple enclosure stacking to a modern material access and invocation, and the utilization efficiency of space has greatly improved. Shelves now fall into three main categories: assembled, integral, and integrated.

A cold-formed thin-wall opening multi-rolled edge ohmic column is the typical design of a steel shelf construction (Fig.1a), which maximizes material performance and improves local buckling bearing capacity. However, continual alterations to the steel structural system of storage shelves, such as multi-high-rise shelves, double-deep shelves, and integrated stereoscopic storage shelves have created new demands on the classic single-leg ohmic column form.[1][2][3][4] Simply increasing the thickness of the column members can improve the structure's bearing performance, but it cannot fundamentally fix the problem, and it will cause the size of the column members and other elements to vary, resulting in intricate operations. And the columns that need to be improved frequently have only a percentage of the area or height, so merely raising the thickness of all columns will increase the cost burden.

There are now engineering efforts in the industry to improve the shelf's column shape and innovatively change the single-leg ohmic column into a double-leg composite column form consisting of two long and short ohmic columns, resulting a novel column section (Fig.1b). The advantage of this arrangement is that it allows for full use of the column space perpendicular to the direction of the roadway while not taking up shelf storage space. At the same time, improve the shelf column's bearing capability. However, this portion has not been thoroughly tested or studied theoretically, and experts and academics at home and abroad are currently focusing mostly on the typical cold-formed thin-wall multi-wound ohm column, with minimal research on the two-limb superimposed column. [5][6][7]

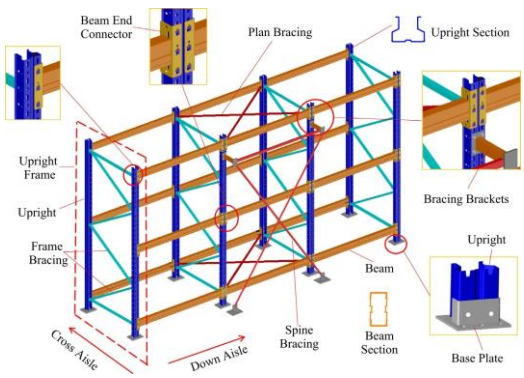

(a) Cold-formed steel storage rack schematic diagram

(b) A two-limb superimposed column used in practical engineering

Fig. 1 Cold-formed thin-wall fabricated rack

Yasar Pala [8] explored the structural performance of cold-formed thin-wall steel rack columns, focusing on enhancing their buckling resistance. The study involved testing and finite element analysis of columns with varying heights to determine critical buckling loads and section sizes. Michael Davies et al. [9] assessed column performance using both finite element analysis and ordinary beam theory (GBT), introducing the "equivalent thickness method" to simplify the modeling of column openings. This approach provides a more accurate representation of the column's behavior under load. Shanmugam et al. [10] developed formulas to assess the impact of different opening shapes (square, circular, and proprietary) on column capacity. Their finite element model considered web slenderness, opening geometry, and proposed that web slenderness and opening area ratio are key variables affecting column performance. Freitas et al. [11] conducted short column tests to establish the bearing capacity of open-hole columns, aligning with standards set by the American Shelf Manufacturing Association and the American Iron and Steel Institute. ANSYS software was used to analyze material and geometric nonlinearities, with results compared to empirical data. Moen et al. [12] presented a simplified method for estimating buckling loads in open-hole columns and

beams of cold-formed thin-wall steel shelves. The study investigated the mechanical properties of columns with variable web openings, considering local, distortional, and global buckling modes, as well as ultimate and failure strengths. Baldassino et al. [13] performed extensive tests (48 axial compression and 24 bidirectional bending) on both perforated and solid sections. They proposed schemes to evaluate the effective second moment of area, addressing gaps in standard specifications and highlighting the influence of opening geometry on column performance. Talebian et al. [14] proposed a finite element model to determine the biaxial bending capacity of cold-formed steel shelf columns. The model accurately replicated published test data and was used for parametric analysis, providing insights into design optimization. Ren et al. [15] used computational methods to investigate the deformation-global buckling interactions in cold-formed steel porous columns under axial compression. The finite element analysis was validated against the direct strength method (DSM), offering a robust framework for design and analysis.

A new sort of column construction is currently being used in real projects, but it has not been extensively analyzed and assessed using numerical simulation, and it is merely installed and welded empirically, with uncertain ramifications for structural safety. Furthermore, the household shelf structure was started late, research on the mechanical performance of the new steel shelf column is still in its early phases, and the theory and standards that can be utilized in practical engineering are still developing. The absence of standardized and appropriate design and processing will also result in a waste of economic and time resources for businesses. As a result, this paper will conduct experimental research on the mechanical properties of commonly used cold-formed thin-wall multi-rolled edge ohm columns and improved two-legged superimposed columns in order to gain a better understanding of their properties and mechanical conditions, as well as provide guidance for engineering applications.

2. Experimental research

2.1. Material properties

This test employed Q345B steel that had been cold bent at the factory. The steel was bent repeatedly to form different corners and stiffeners. The cross-sectional shape was complex, and the bearing capacity was large. The column material used for the material test must be from the same batch of steel as the bearing capacity test. It should be cut during the rolling process of the steel plate, with the direction perpendicular to the rolling direction. The specimen material is processed into a plate-shaped lead specimen in accordance with the provisions of standard GB/T 228.1-2021 [16]. Three identically sized standard plates were given to each group of specimens (Fig.2), and each specimen was subjected to uniaxial tensile testing at room temperature in compliance with EN 15512-2022 [17] standard. Table.1 displays the test results.

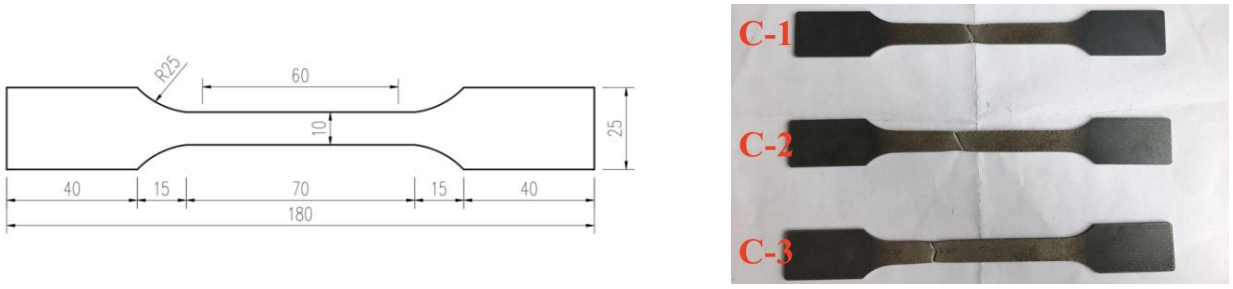

(a) Size diagram of material performance test specimen (b) The final failure mode of the material performance test specimen

Fig. 2 Schematic diagram of material performance test specimen

Table 1
Results of material performance test

Specimen	Specimen Number	Yield Strength $f_y(MPa)$	Average Value $f_y(MPa)$	Plastic Stress ε_{pl}	Tension Strength $f_t(MPa)$	Average Value $f_t(MPa)$	Plastic Stress ε_{pl}
Column	C-1	352	363	0	447	453	0.016
	C-2	365			453		
	C-3	371			460		

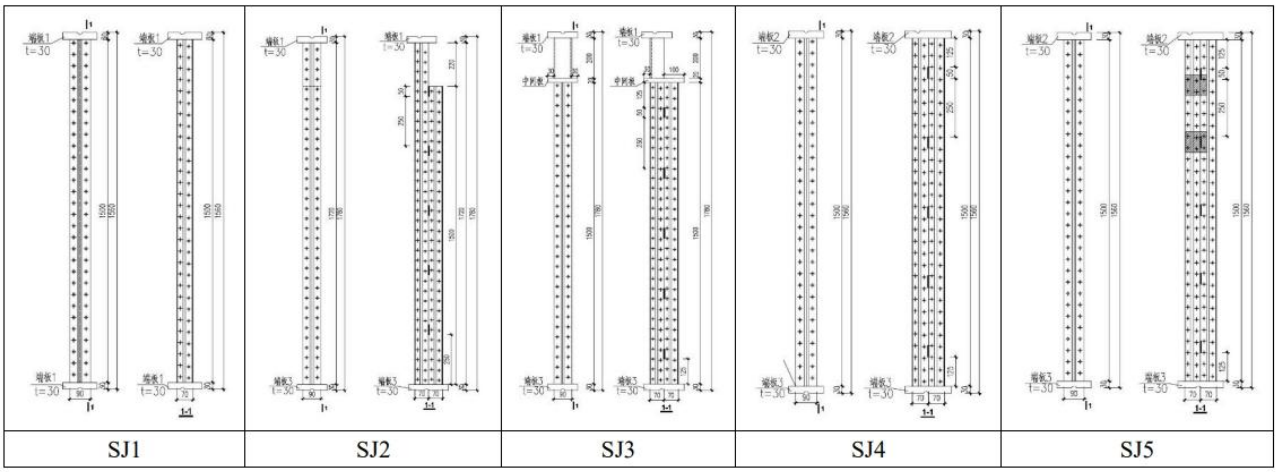

Fig. 3 Specimen diagram

2.2. Specimen design

The column specimens（Fig.3）are divided into five types. The first type of SJ1 column is a single-limb ohmic column. The N90 segment, which is extensively utilized in the market today, is used. The specimen is 1500 mm long and has 150 × 150 × 30 mm end plates welded at the upper and lower ends to

accommodate the test device's height and space limits.

The second type of SJ2 column is a double-limb laminated column, which was employed in the project. The single-limb ohmic column is converted into a double-limb laminated column by immediately splicing a long (1720mm) and a short (1500mm) ohmic column, resulting in a closed superposition of an open cross-section column. There is no force plate between the long and short transition zone. The upper end is welded with a 150 × 150 × 30mm end plate, while the lower end is welded with a 200 × 150 × 30mm end plate.

The third specimen, SJ3, is an optimized version of SJ2. The preliminary test demonstrated that the ohm column on the upper half of the transition portion of the SJ2 column is susceptible to distortional buckling, resulting in a reduction in ultimate bearing capacity. To prevent distortional buckling of the upper portion, the SJ3 column is divided into two sections: upper and lower. The upper part consists of three 6 mm composite plates enclosed by a 200-mm-high short column. The centroid position is same to that of the single limb ohm column. The central transition part has a 200 × 150 x 20 mm thick force transmission plate. The lower part is a double-limb composite column joined by two 1500 mm single-limb ohm columns. The splicing component is welded discontinuously, causing the top short column and outer limb column of the lower double-limb composite column to overlap. The upper end is welded with 150 × 150 × 30 mm end plate, while the lower end is welded with 200 × 150 × 30 mm plate.

The fourth specimen SJ4 simplifies the specimen JS3 by removing the upper short column and replacing the middle force transmission plate with a 30mm thick force transmission end plate. The upper and lower ends are welded with plates measuring 200 × 150 × 30mm.

The fifth specimen, SJ5, has a batten plate attached to both sides of specimen SJ4. The batten plate measures 96 × 90 × 5 mm. Two layers are welded together, with one layer consisting of the batten plate's two sides that have the same height. The center of the first batten plate layer is 150 mm from the bottom of the top end plate, and the second layer's center is 400 mm from the same place. Welding secures the batten plate to the column.

2.3. Test setup and process

The mechanical performance of the cold-formed thin-walled constructed shelf column was assessed at the structural laboratory at Nanjing University of Aeronautics and Astronautics. The test platform is a 200t bidirectional loading test bench capable of withstanding loads ranging from 0 to 200 t. By reviewing the research methodologies of researchers at home and abroad, [18][19][20] it is discovered that the use of hinged ends can eliminate the majority of the end limitations, allowing the test to more closely imitate the true stress of the column in the real project.

Given the stress situation of cold-formed thin-walled assembly shelf columns in engineering practice, the specimen SJ1 column's bearing capacity test uses the column's axial compression test technique. The remaining parts are double-limb stacked columns. In engineering practice, the compression test scheme is used with the upper loading point as the center of the outer limb column and the lower connection point as the center of the double limb superimposed column. The column compression test loading device is basically made up of a two-way hydraulic jack, a pressure sensor, end spherical hinge support, a support platform, and other components. The bottom support of the column loading device is made up of the end spherical hinge support, steel ball, and support platform, which are bolted together. Fig.4(a) displays the schematic diagram of the loading device and the support.

The bearing capacity test primarily uses the load and displacement of the two primary mechanical parameters to determine the column's mechanical qualities. The vertical displacement primarily measures the displacement of the upper and lower end plates, but it also determines the column's vertical compression displacement and the end plate's rotation angle. The horizontal displacement primarily measures the deformation of the column section.

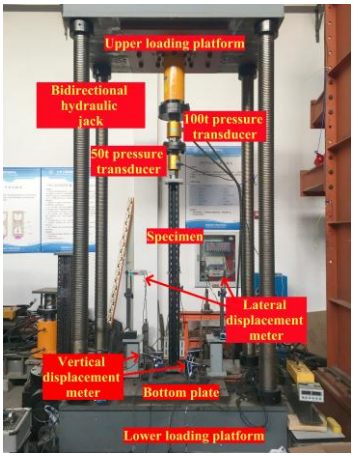

(a) Loading device of load test

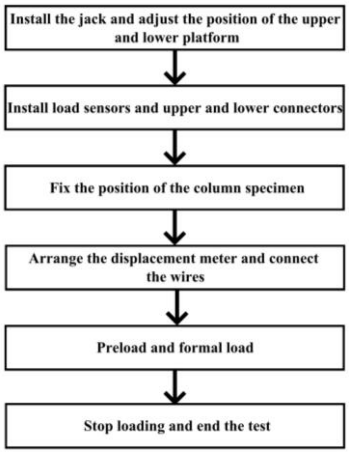

(b) Flow diagram of test loading

Fig. 4 Loading device and flow diagram

During the test, the jack must be installed and the upper and lower platforms' positions adjusted. The column specimen is then put in position, the displacement meter is set up, and the wire is connected, followed by the loading test and data collection. The specific test process is shown in the Fig.4(b). The DH3816 static strain test system automatically collects and summarizes data from the load sensor and displacement meter in all directions.

2.4. Analysis of test failure results

The test involved loading five different types of columns and six specimens. (Because the first test column may contain test mistakes such as misalignment and measurement problems, two SJ1 specimens with the same cross-section size were created, designated SJ1-1 and SJ1-2). Because the test conditions for each column varies, this section discusses the test phenomena for each specimen separately. The test data is collated and calculated to generate several load curves, and the variations in each curve are examined.

2.4.1. Single limb Ohm column SJ1

Fig. 5 shows the failure modes and load-displacement curves for specimens SJ1-1 and SJ1-2. The vertical compression displacement of the upper and lower end plates is measured at four corner points to provide more precise data; the average value is selected as the final value. When the load is first applied to the column, it is proportional to the axial displacement, which rises with the load. Nevertheless, the displacement rises and the load growth rate falls when the load approaches the ultimate load range, or when the load approaches 70% of the ultimate bearing capacity. The two are disproportionately huge. The column begins to plasticize, and the plastic hinge appears on the failure portion. Local bending occurs at the claw hole in the center of the SJ1-1 web, causing the specimen to shift to one side. The distortional buckling starts at the central flange of SJ1-2 and moves slightly to the exterior. When the load exceeds the ultimate bearing capacity range, the load and axial displacement rapidly decrease until they approach the critical value or failure condition. The central section of the specimen SJ1-1 was noticeably twisted, and there was noticeable local buckling at the web claw hole. The test was finished after the central part of specimen SJ1-2 demonstrated evident distortional buckling.

The two single-limb ohm columns SJ1-1 and SJ1-2 rotate in both the X and Y axes, but the Y axis rotation is modest, while the X axis rotation is very noticeable. The load-rotation curve is given in Fig.6. During the initial loading stage, the upper and lower end plates rotate minimally, with no visible difference. The specimen's angle remains rather consistent across the range of final bearing capacity, with no discernible rotation at the upper and lower ends. The angle around the X axis gradually increases after exiting the range of

ultimate bearing capacity, and it is evident that the upper and lower end plates rotate. The rotation angle varies between 1.0° and 3.0°, and the total angle around the X axis, which is the sum of the angles of the upper and lower end plates, is 5.0°.

The column's load-lateral displacement curve describes the change in cross section at maximum deformation. The two single-leg ohm columns distort most significantly around the middle. When setting the lateral tie rod type displacement time, a positive value on the displacement meter indicates that the tie rod is pushed back, implying that the plate of the column section is bulging or bending outward; a negative value indicates that the tie rod is extended. The plate of the column section is concave, meaning it curves inward. Depending on the location of the measurement point, the displacement meter at each position shows the deformation of various regions. The single limb ohm column's flange deformation is measured by displacement meters Nos. 9 and 14. While Nos. 11 and 12 displacement gauges show section web deformation in the center of the column, Nos. 10 and 13 show flange distortion at the web surface in the middle of the column（Fig.7）.

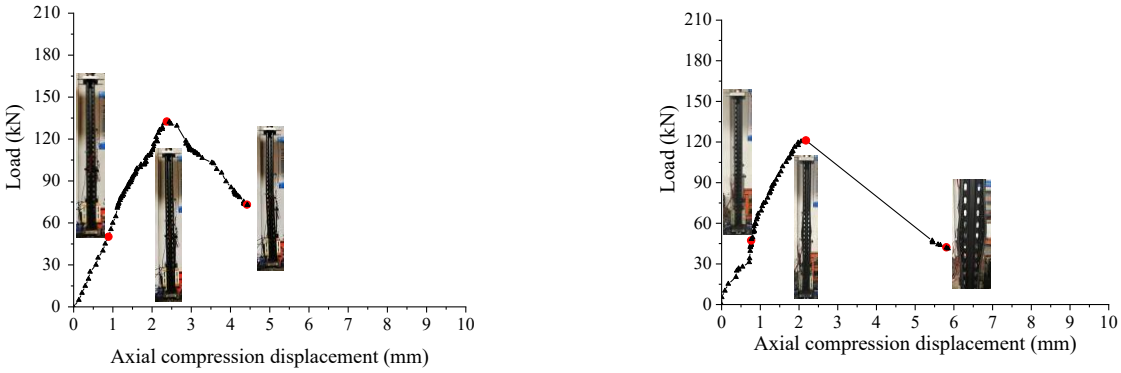

(a) SJ1-1 (b) SJ1-2

Fig. 5 Load-axial compression displacement curve of specimen SJ1

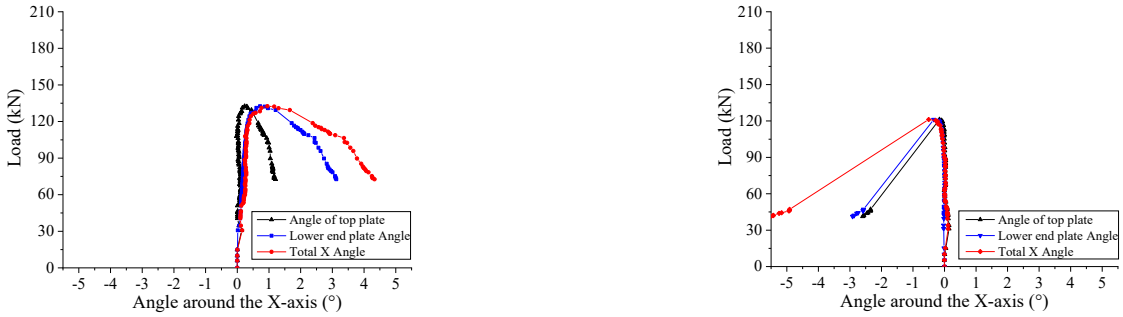

(a) SJ1-1 (b) SJ1-2

Fig. 6 Load-angle curve of axial compression specimen

The distortion and buckling of the center half of the two single-limb ohm columns happened first, followed by the appearance of the specimens' plastic hinges and, to some extent, overall instability. The load's lateral displacement. The angle curves of the two single-limb ohm columns are generally compatible with the test findings, indicating the columns' overall instability. When the load exceeds the column's maximum bearing capacity, the deformation speed of the central component accelerates, emphasizing the column's overall instability.

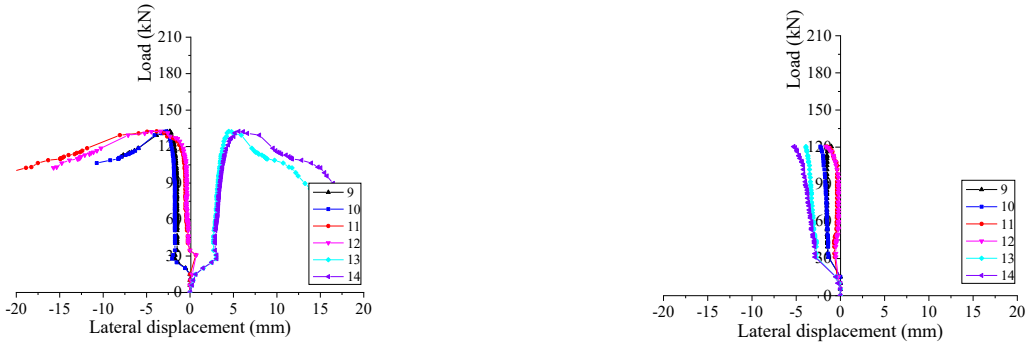

(a) SJ1-1 (b) SJ1-2

Fig. 7 Load-lateral displacement angle curve of axial compression specimen

2.4.2. Double limb ohm column SJ2-SJ5

Fig.8 shows the load-vertical displacement curve for SJ2-SJ5. The double-limb composite column has significantly more bearing capacity than the single-limb column. At the start of loading, the load is proportional to the axial displacement, which increases as the load increases. But when the load approaches 80% of the ultimate bearing capacity or enters the zone of ultimate load, the displacement rises while the load growth rate falls, and the two are not equal. The plastic hinge appears on the failure area as the column starts to plasticize. The load and axial displacement rapidly decrease and swiftly reach the critical value or failure situation when the load is outside the range of ultimate bearing capacity. This marks the end of the test.

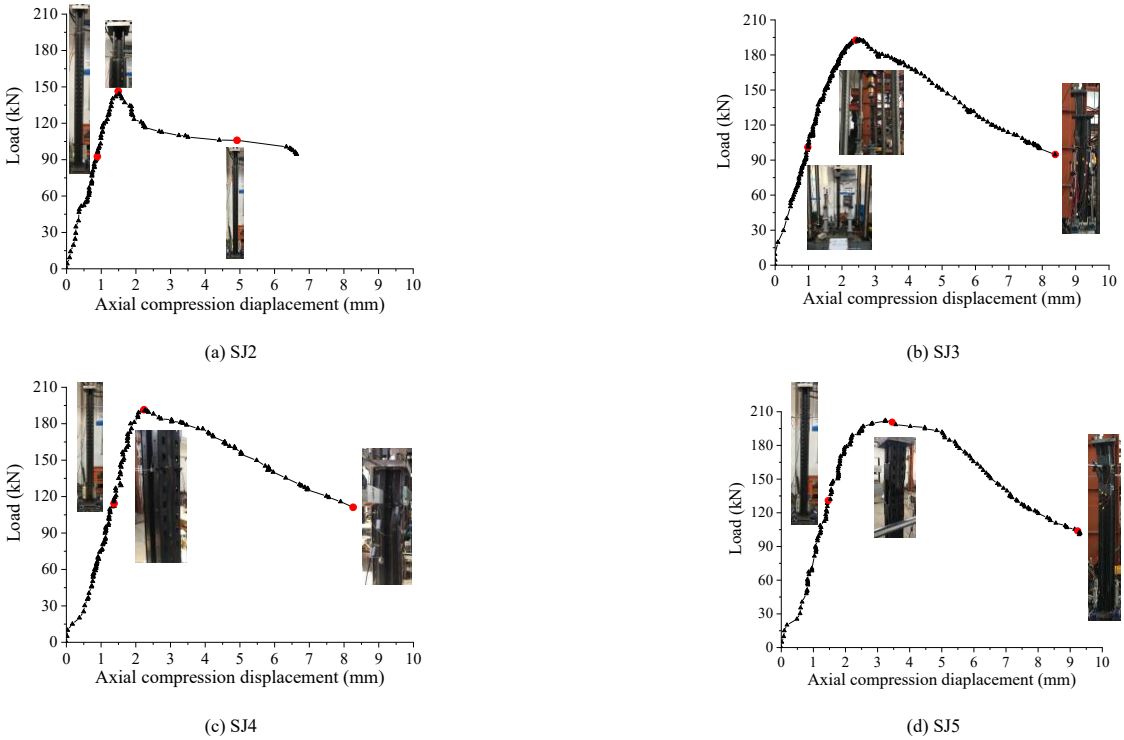

(a) SJ2 (b) SJ3

(c) SJ4 (d) SJ5

Fig. 8 Load-axial compression displacement curve of double-limb composite column

The mechanical performance of the outer limb ohm column has the greatest influence on the bearing capacity of the SJ2 column used in this project. Its bearing capacity is not considerably higher than that of a standard single-limb cold-formed thin-walled column, and it is reduced due to the eccentricity. With an intermediate transition plate, the SJ3 column's bearing capacity has significantly enhanced. When the column height, position, and direction of the loading point on the upper end plate are all the same, the SJ3 section's bearing capacity is 31.4% greater than that of the SJ2 section.

During the bearing capacity test, all of the double-limb composite columns were rotated to varying degrees around the X/Y axis, with the X axis being the most visible. As a result, the system's data will be calculated and processed to generate the load-rotation curve of the four double-limb composite columns around the X axis (Fig.9). Column SJ2's total rotation angle around the X-axis is opposite that of the other three columns. The SJ2 column end plate rotates around the X-axis at a negative angle, whereas the SJ3, SJ4, and SJ5 end plates rotate positively. The bottom end plate of the column rotates at a small angle (± 0.5 °), whereas the higher end plate rotates the most. When the specimen reaches the ultimate load and is destroyed, the one with the SJ4 section has the greatest angle of rotation. The SJ4 and SJ5 sections' rotation angle changes very little in the first stage, suggesting that the displacement meter's sensitivity is low at the beginning of the loading stage and that the section's rotation angle does not change significantly. The lower end plate rotates along the X-axis in the opposite direction before turning in the positive direction when the load hits 20kN, causing a significant shift in rotation angle.

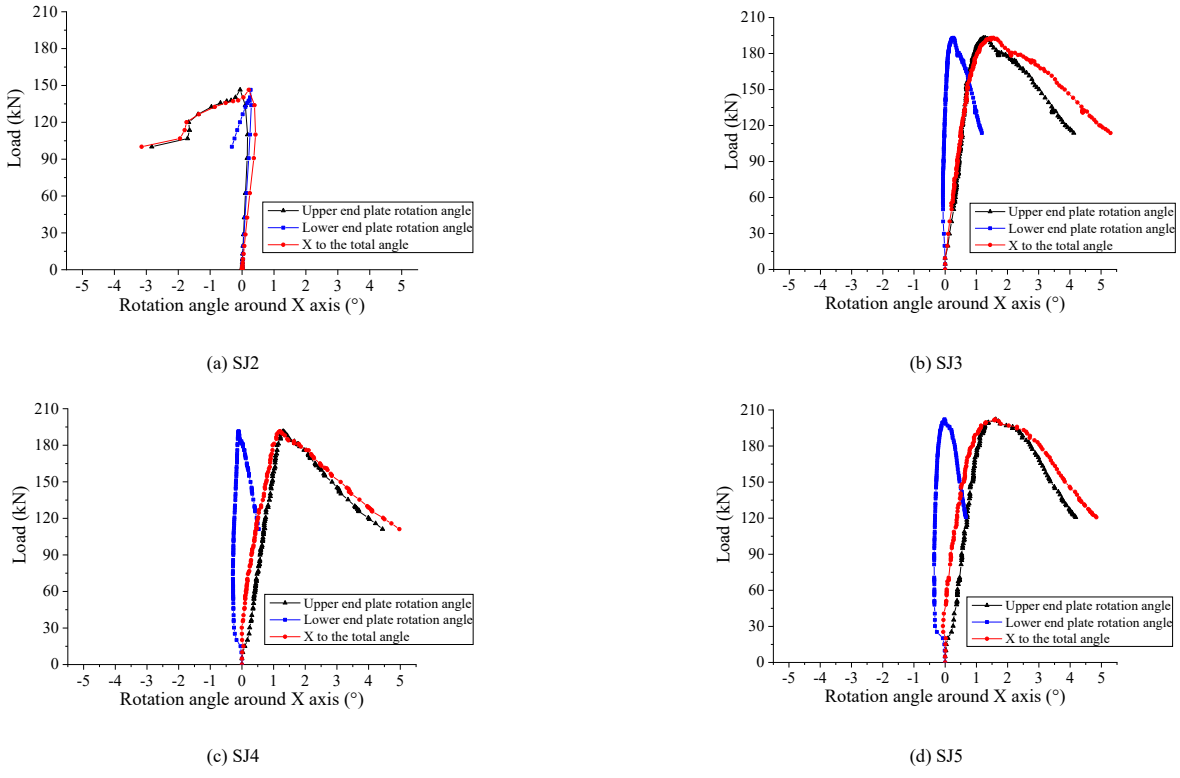

(a) SJ2 (b) SJ3

(c) SJ4 (d) SJ5

Fig. 9 Load-rotation curve of double-limb composite column under compression

The load-lateral displacement curve for the four column specimens is shown in Fig. 10. The variation law of the curve in the figure is broadly consistent with the test procedure: the column SJ2 does not change appreciably before the load is applied to the final bearing capacity. The displacement at the deformation increases quickly after reaching the maximum bearing capacity, which is broadly consistent with the test's findings. The displacement values obtained by symmetrical measuring locations in the other three columns' load-lateral displacement curves are essentially the same, implying that the shapes and changes of No.9 and No.14, No.10 and No.13, and No.11 and No.12 curves are all consistent. The local buckling failure deformation of the column is also symmetric around the symmetry axis. Consistent with the field test results, the displacement range of the No. 11 and No. 12 curves is significantly larger than that of the other four displacement meters, indicating that the outer column web is more severely deformed than the flange.

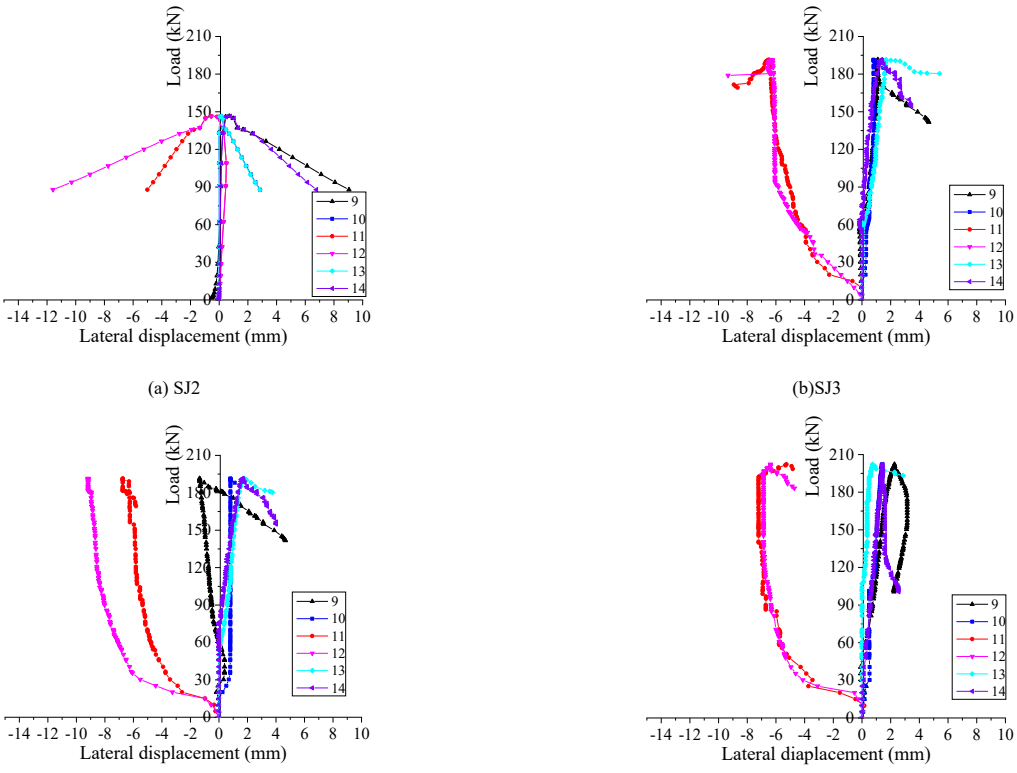

(a) SJ2 (b)SJ3

(c) SJ4 (d) SJ5

Fig. 10 Load-lateral displacement curve of double-limb composite column under compression

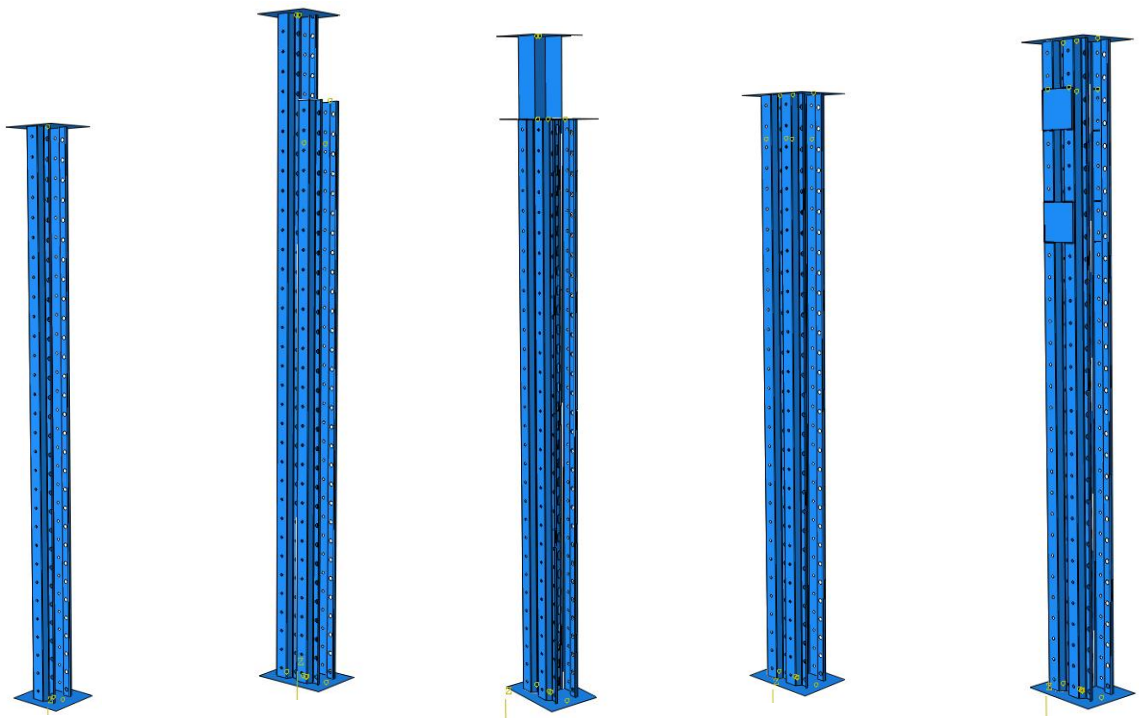

(a) SJ1 (b) SJ2 (c) SJ3 (d) SJ4 (e) SJ5

Fig. 11 Finite element model of column specimen

3. Finite element analysis

This chapter uses the finite element program ABAQUS to examine the mechanical properties of a cold-formed thin-walled assembled shelf column. The software compares numerical simulation results to the experimental results and investigates stress distribution and column deformation during the stress process are examined [25]-[30]. The model's perspective is used to explain the fundamental notion of column force change, as well as the essential aspects that may affect the mechanical performance of the cold-formed thin-walled constructed shelf column.

3.1. Finite element model

This research focuses on cold-formed thin-walled steel members. In this paper, the columns, end plates, and batten plates are modeled and analyzed using the general shell element S4R (4-node quadrilateral finite film strain linear reduction integral shell element), which has the best performance and is extensively used in the ABAQUS software element library.

Because the cross-section curling of the commonly used cold-formed thin-walled steel shelf column is difficult, the drawing function in AutoCAD must be utilized to create the cross-section of the ohm column. The software's stretching function transforms the cross-section into a three-dimensional entity, after which the column is opened with a Boolean operation. When the column member is completed, the component module is imported using the ABAQUS software's import system, and the whole column component is received. The remaining components, such as the batten plate and end plate, are imported in the same way. Fig.11 shows the finite element model for the five column specimens under test.

The nominal stress and strain of elastoplastic materials are determined directly from the material performance test. However, the material's actual stress and plastic strain must be mentioned in the ABAQUS material definition. As a result, the nominal stress and strain received from the material property test must be converted into real stress and plastic strain (Table.1). In ABAQUS, section characteristics with containing material attributes are first established and then assigned to each area of the overall model to describe component material properties.

The component's initial geometric defects are introduced utilizing the consistent defect mode [21][22] technique in conjunction with the buckling form of the test findings, as investigated in this study. Scholars, both domestic and international, use the technique's relatively simple and workable approach. In the simulation study of this article, the amplitude value of various starting defects may be used to derive the load displacement curve and ultimate load of the specimen when combined with GB50017-2017 [23] and EN1993-1-5 [24]. A minor amount of residual stress will be created during the specimen processing, however the effect of taking residual stress into account is more complicated, hence the effect is not taken into account in the finite element model used in this work.

Each node in the ABAQUS program has six matching degrees of freedom that can be controlled. The real state of the node can be duplicated by defining or limiting the degrees of freedom associated with it. The hinge point in this simulation initially situated on the end plate, and its six degrees of freedom are controlled and restricted. The higher end of the column can be used to simulate a test jack by limiting UX and UY's degrees of freedom at the upper end plate's loading location. The specimen's flat east in the Z direction and the column's rotation in the X, Y, and Z directions. The four degrees of freedom of UX, UY, UZ, and ROTZ are thus limited at the lower end plate's hinge point, allowing the lower end plate to rotate solely in the X and Y planes.

When changing the grid control properties, the unit shape is changed to quadrilateral to reduce grid distortion and improve simulation computation convergence. The neutral axis algorithm is then utilized to choose the minimum grid transition to divide the grid freely. The grid is divided according to the norm that the approximate global size of the column member is 8 mm, and the approximate global size of the end plate and batten plate member is 5 mm, when the grid size is established in accordance with the empirical law of the research group's previous simulation. Fig.12 shows the divided mesh model.

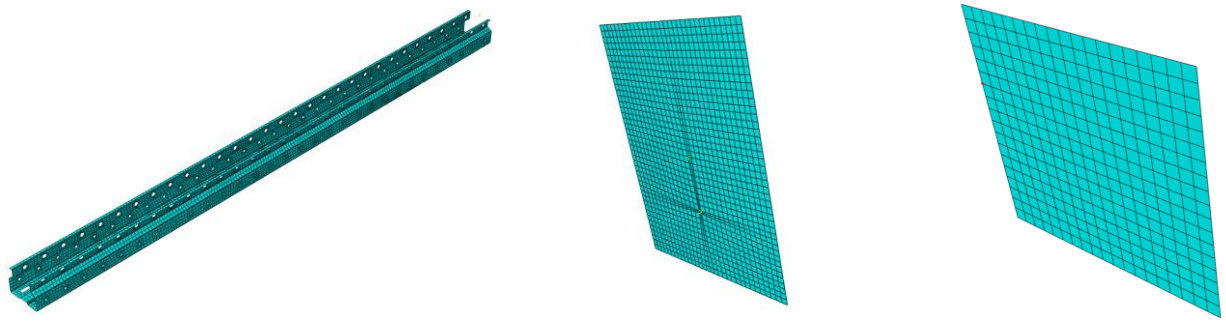

(a)The column (b)The end plate (c)The batten plate

Fig. 12 Meshing Shape of Column Components

3.2. Finite element simulation analysis

The finite element simulation in this study employs nonlinear buckling analysis, allowing the deformation of the section entering the post-buckling stage to be calculated. In the finite element simulation, 60% of the ultimate load is used as the critical value, and the calculation is terminated when the load surpasses the ultimate load and reaches the critical value. The simulation result represents the final deformation. The load-displacement curve generated from the simulation calculation is compared to the experimental result (Fig. 13). The overall trend is relatively constant, and the slope of the initial stage is nearly identical.

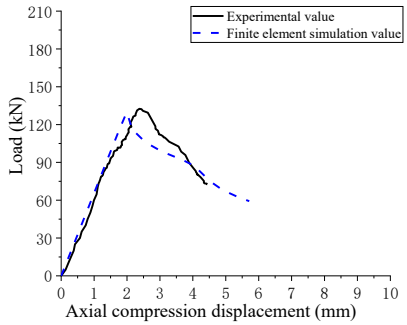

(a) SJ1-1

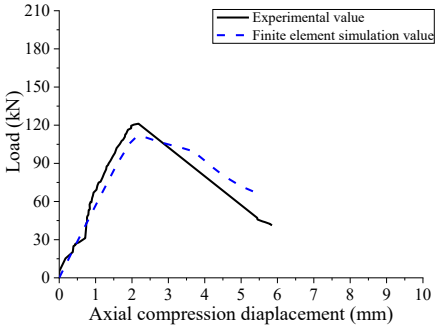

(b) SJ1-2

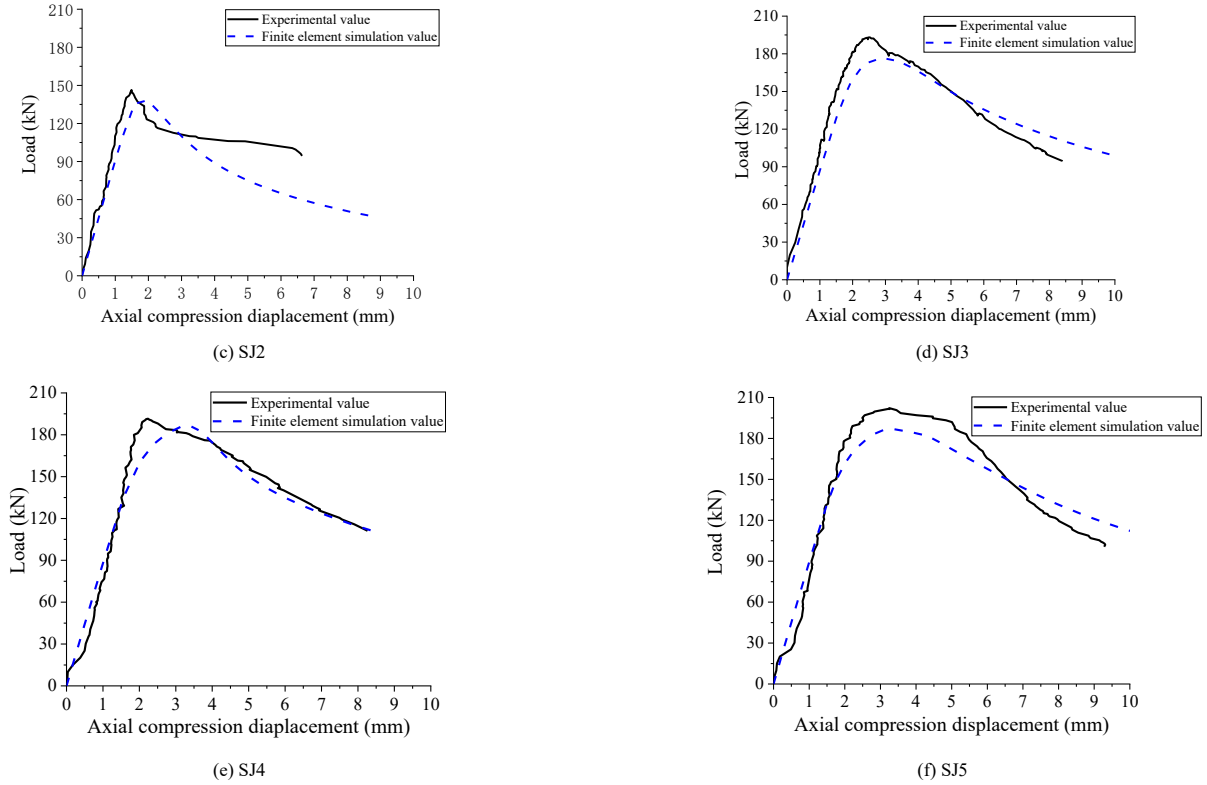

(c) SJ2 (d) SJ3

(e) SJ4 (f) SJ5

Fig. 13 Finite element results of load-axial compression displacement curve

The compressive specimens of the single-limb Ohmic column have various degrees of rotation in the X and Y axes, whereas the compressive specimens of the double-limb composite column primarily rotate in the X axis. The curves of various columns are summarized using the rotation angle around the X axis, and the finite element and experimental data are compared and examined (Fig.14). The experimental and finite element values of the load-rotation curves of all column specimens are nearly identical; the initial slope of the test curve is greater than the initial slope of the simulated value curve, indicating that the rotation speed of the test value is slow at the start of the rotation angle. The test findings demonstrate that the rotation process is caused by the spherical hinge's non-ideal state. The rotation is limited by a certain amount of resistance.

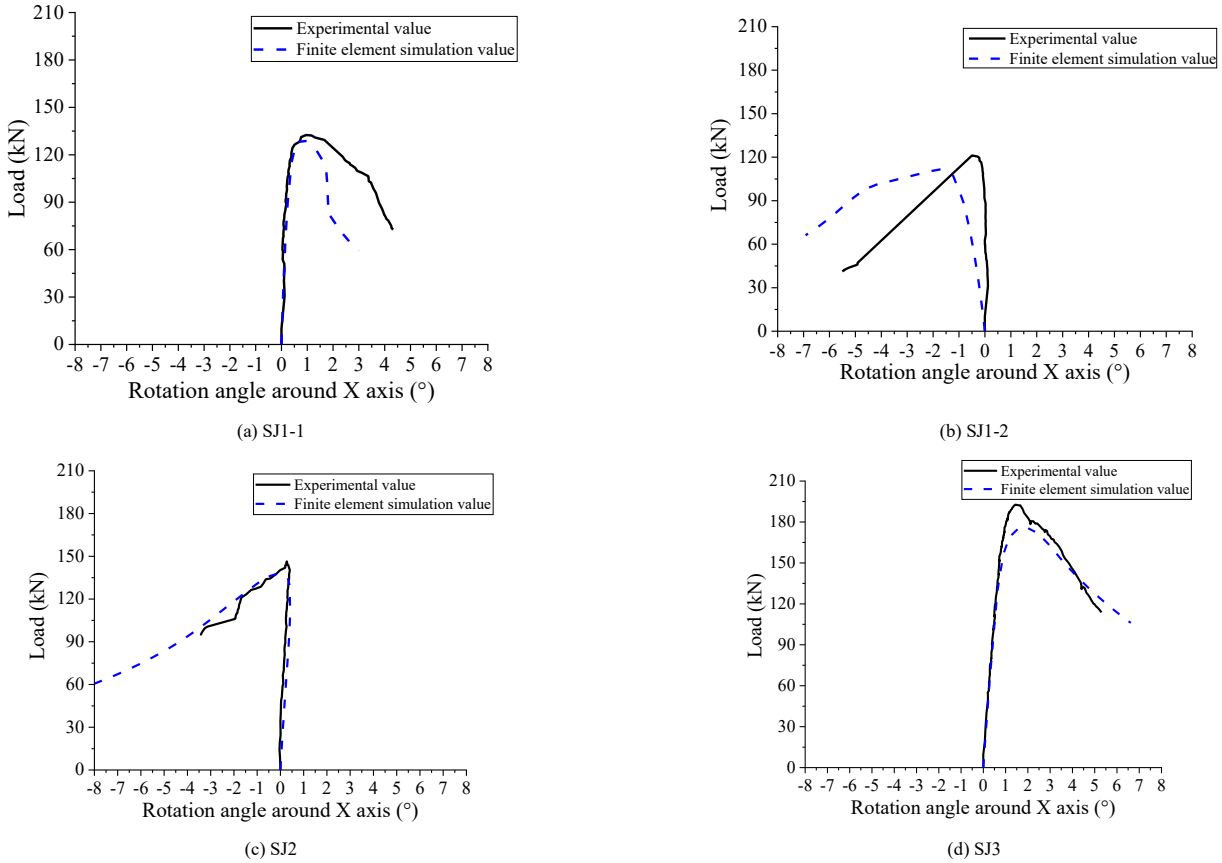

(a) SJ1-1 (b) SJ1-2

(c) SJ2 (d) SJ3

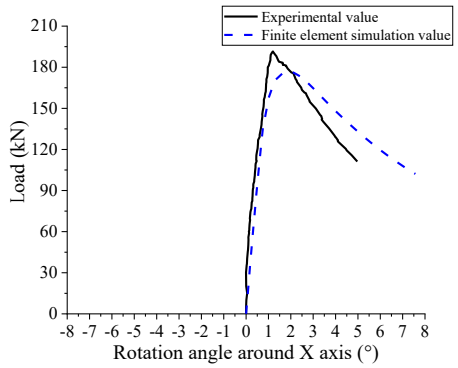

(e) SJ4

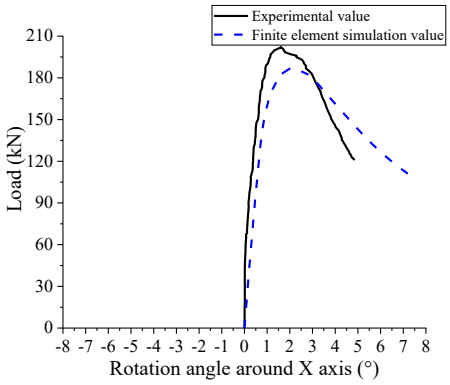

(f) SJ5

Fig. 14 Finite element results of load-rotation curve

3.3. Ultimate capacity analysis

In addition to comparing and assessing experimental and finite element values, a finite element model without starting flaws is created for computation, with the understanding that adding initial faults results in a lower finite element simulation value. The ultimate bearing capacity value P0 is compared to the experimental value PT and the finite element value PFE. The results are shown in Table.2.

Table 2
The column test results are compared with the finite element analysis results

Classification	Specimens Number	Mode of Failure (D: Distortional buckling; L: Local buckling)		Ultimate Bearing Capacity			Error/% $(P_T - P_{FE})/P_T$
		Test	Finite Element	P_T/kN	P_{FE}/kN	P_0/kN	
Single Limb Column	SJ1-1	D	D	132.54	129.77	131.36	2.08
	SJ1-2	D	D	121.19	111.86	115.31	7.70
Double-leg column	SJ2	D	D	146.42	137.84	141.56	5.86
	SJ3	L	L	192.69	176.02	183.64	8.64
	SJ4	L	L	191.49	177.11	188.28	7.51
	SJ5	L	L	202.24	186.90	195.70	7.59
		Average Error					6.56

The table demonstrates that the final failure modes of each column specimen in the test and the finite element simulation results are virtually identical. In this test, the variation between column test and simulation results ranges from 2% to 9%. The test value for each column's ultimate bearing capacity exceeds the simulation value. The lowest error is 2.08% in the single-limb ohmic column SJ1-1, the worst is 8.64% in SJ3, and the average is 6.56%. The error is within the acceptable range.

By developing a better finite element model of the shell element, column tests can be replicated more precisely. A set of load displacement curves can be created by converting and computing the data from the finite element simulation results.

4. Research on the influence of parameters

When the finite element simulation results are compared to the real test results, they are almost identical, demonstrating that the column may be successfully simulated if the column section is carefully drawn and the finite element parameters are properly specified. In this chapter, the SJ4 cross-section column (cold-formed thin-walled constructed double-limb composite column) is used as the main model, and more parametric research is carried out on its foundation.

The slenderness ratio of the column(λ), the number of batten plates(n), the thickness of the column(t_c), the length(l)and spacing of the discontinuous welds(d) , and the thickness of the dowel plate(t_d)will all have an impact on the ultimate bearing capacity and failure mode of the cold-formed thin-walled assembled double-limb composite column. The preceding test and finite element analysis results indicate that the column's slenderness ratio will influence the component's final failure mode.

When $\lambda \leq 85$, the final failure mode is local buckling failure. The failure section consists mostly of the column's middle and upper parts, with the upper end plate rotating along the X axis. When $85 \leq \lambda \leq 95$, the specimen's final failure mode is between local and overall buckling failure. The column's failure is influenced by both buckling modes. When $\lambda \geq 95$, the specimen's final failure mode becomes general instability failure, with increased lateral bending increases. The column's failure point is predominantly located in the middle, with no significant change near the ends.

The increase in batten plate has a more evident positive influence on local buckling instability. Welding the batten plate to the column's local buckling failure can increase the final bearing capacity by around 5% while also boosting the region's cross-sectional strength. Furthermore, expanding the batten plate can have a more noticeable impact on the column's local stability, but the effect on the column's overall stability is unknown.

The following three influencing factors will have a substantial impact on the cold-formed thin-walled assembled double-limb composite column's ultimate bearing capacity and failure mechanism. As a result, in order to accurately analyze the specific change process of each influencing factor on the column, as well as provide the influence law and related suggestions for each key factor, a detailed parametric analysis of the double-limb composite column is required to lay the groundwork for the column's research and design in the project.

4.1. Thickness of column(t_c)

The average thickness of a steel shelf structure in industry is between 2.0 mm and 3.5 mm. When the thickness is less than 2.0 mm, the column's bearing capacity rapidly drops, resulting in reduced safety performance. If the thickness is too large for cold-formed thin-walled steel members, the difficulty of cold-formed rolling of thick plates in the factory will skyrocket, and when the material thickness exceeds 3.5mm, the section will be more likely to produce fine cracks after cold bending, which is detrimental to structural safety and negates the economic benefits of cold-formed thin-walled members.

Based on the specimen SJ4, this portion selects component heights H = 1.5m to ensure that the remaining test conditions are identical to the previous ones. The specimen's boundary conditions are changed so that it can hinge at either end. The spacing between the intermittent welds is 300mm, and their length is 50mm.Change the thickness of the component's column and generate a collection of finite element parametric models for analysis.

The simulation results in Fig.15 clearly show that the ultimate bearing

capacity of the double-limb composite column gradually increases as the column's wall thickness increases, which is essentially linear; however, the column's final failure mechanism is independent of wall thickness.

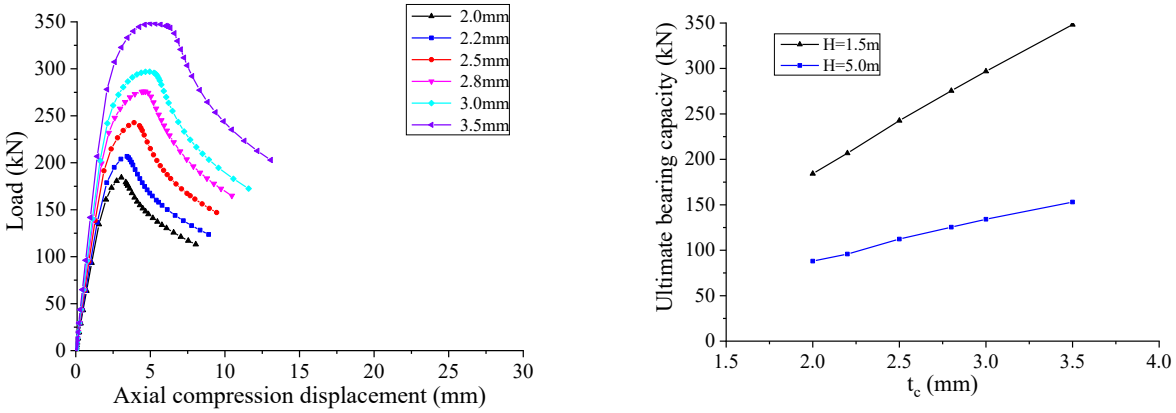

(a) Load-axial displacement curves of specimens with different column thicknesses

(b) Comparison curves of ultimate bearing capacity of specimens with different wall thicknesses

Fig. 15 Analysis of the influence of column thickness

Table 3
Intermittent weld parametric model specification table

l(mm)	d(mm)	No.
10	750	HF10-1
	500	HF10-2
	300	HF10-3
30	750	HF30-1
	500	HF30-2
	300	HF30-3
50	750	HF50-1
	500	HF50-2
	300	HF50-3

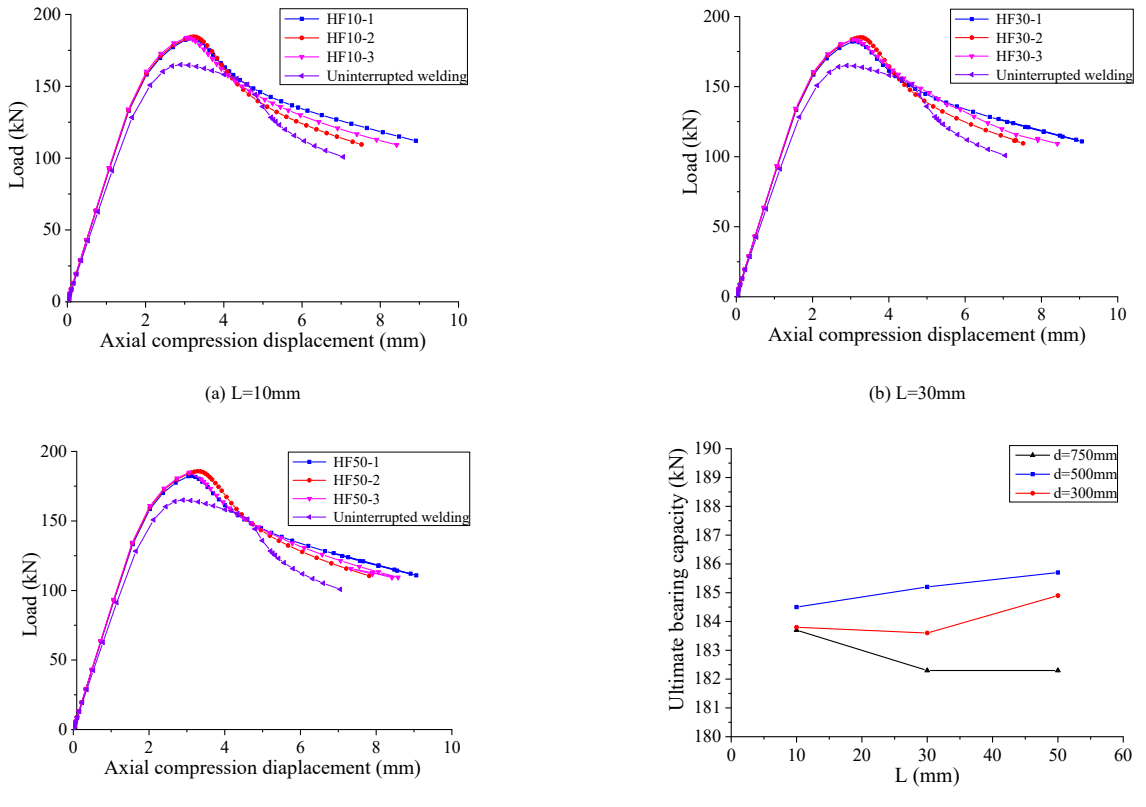

(a) L=10mm

(b) L=30mm

(c) L=50mm

(d) Ultimate bearing capacity of weld parameters at different heights

Fig. 16 Analysis of the influence of weld length and spacing

4.2. Column weld length(l) and spacing(d)

The load test and finite element simulation analysis of the cold-formed thin-walled assembly shelf column under consideration in this study show that there are no fixed standards or specifications, and the length and intermittent weld spacing are empirical values. The estimated values from the project are used in the preceding test and finite element analysis. In terms of cross-section, the intermittent welding between the inner and outer limb columns provides the primary support for the double-limb composite column based on SJ4. Thus, in this section, we will look at the bearing capacity of the cold-formed thin-walled assembly shelf column, as well as the effects of modifying the weld spacing and intermittent weld length.

The components are divided into three groups based on their weld length: 10 mm, 30 mm, and 50 mm, in that order. The weld spacing changes from large to tiny under the left and right symmetrical intermittent welding arrangements, depending on the type of weld length. The column is 2mm thick, and the other properties are identical to those of the SJ4 section. Table.3 shows the individual model parameter changes.

As seen in Fig.16, it is:

(1) When the weld spacing is the same, the constructed double-limb composite column's bearing capacity is not improved by the length of a single weld, and the weld's length has no effect on the column's final bearing capacity. The column's bearing capacity is mostly determined by its own bearing capacity.

(2) When the same weld length is utilized, the load bearing capacity rises as the weld spacing reduces. That is, the ultimate bearing capacity of the column increases with a denser surface weld arrangement, but the range of enhancement is limited.

(3) Whether or not there are continuous welds has a considerable impact on bearing capacity. At a 1.5-meter column height and a 750-millimeter weld spacing, the ultimate bearing capacity of weld lengths of 10 mm, 30 mm, and 50 mm is 9.2%, 9.1%, and 9.0% higher than that of the non-welded column, respectively.

(4) The weld configuration varies with the height of the column. The final bearing capacity of the column is greatest and most cost-effective when the spacing between the long column's discontinuous welds is 300 mm and the weld length is 30 mm. The short column's discontinuous weld spacing is best configured at 500 mm, and the longer the weld length, the greater the ultimate bearing capacity.

4.3. Thickness of the dowel plate(t_d)

In the previous test, specimen SJ3 had a 31.4% higher ultimate bearing capacity than SJ2, demonstrating that adding the dowel plate can significantly increase the bearing capacity of the double limb composite column. To fully study the influence of dowel plate thickness on the bearing capacity of the SJ3 section, the column force is measured as the thickness of the dowel plate is varied. The thicknesses of the dowel plates are 2mm, 5mm, 10mm, 15mm, 20mm, 25mm, 30mm, and 40mm, respectively. Aside from the dowel plate, the remaining attributes are equivalent to SJ3. The upper short column is 8mm thick, while the lower double-limb composite column is 2mm.

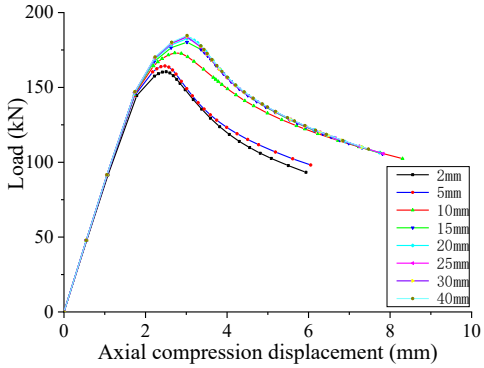

(a)Load-axial displacement curves of specimens with different thickness of force transfer plate

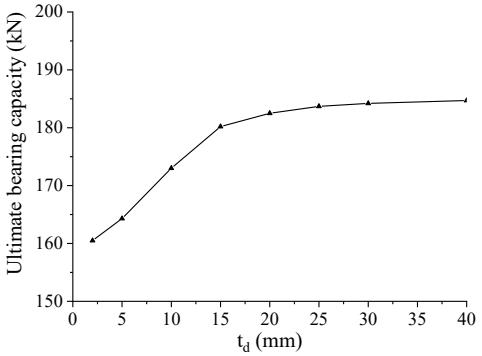

(b)Comparison curves of ultimate bearing capacity of specimens with different thickness of dowel plate

Fig. 17 Analysis of the influence of the thickness of the force plate

As seen in Fig.17, it is:

(1) At the commencement of loading, the load-axial displacement curve for a double-limb composite column with different force plate thicknesses is virtually equal to the finite element model. The ultimate bearing capacity increases with the thickness of the dowel plate, suggesting that increasing the thickness of the dowel plate helps the top structure to distribute the weight more uniformly to the double-limb composite column, allowing the column to withstand greater load.

(2) The thickness of the dowel plate impacts the column's final bearing capacity in several ways. At 0 ~ 20mm, the curve slopes to a straight line, indicating a large improvement in ultimate bearing capacity. At the 20-40mm stage, the slope is gentle, and the column's ultimate bearing capacity increases slowly. For optimal results, choose a dowel plate thickness of 15-25 mm. Because 20 mm is the normal size, it is the most economical to use 20 mm thickness.

5. Conclusions

In summary, the following conclusions can be drawn:

(1) The cold-formed thin-wall double-limb composite column is suited for shelf projects due to its compact design, ease of manufacturing, high bearing capacity, and strong anti-side ability. The two-limb composite column's force performance is higher after application and testing in the actual project, saving cargo storage space in the strong axis while boosting lateral stiffness in the weak axis.

(2) The directly spliced two-limb composite column SJ2 (no force transfer plate) has distortion buckling failure in the test, and the ultimate bearing capacity is improved to some extent compared to the single-limb ohm column, but the co-working performance of the inner and outer limbs of the two-limb composite column is not fully realized. The failure of the two-legged composite columns SJ3 with force transfer plate and composite column, SJ4 with force transfer plate, and SJ5 with force transfer plate and composite plate was caused mostly by local buckling. In comparison to the SJ1 and SJ2 sections, the ultimate bearing capacity is significantly increased. The final bearing capacity of the two-limb composite column can be raised to a certain extent by placing plates on both sides.

(3) The bearing capacity of the two-limb composite column increases with the thickness of the column plate, and the relationship is nearly linear; nevertheless, increasing the thickness does not change the column's final failure mode. Columns with $\lambda \leq 85$ typically fail due to local buckling, primarily in the middle and upper sections of the column. A column with $\lambda \geq 95$will fail due to overall instability, with the failure spot located in the middle. The column section with a thickness of 3.5mm is the most efficient and cost-effective.

(4) The spacing and weld size of the discontinuous welds have no effect on the column's ultimate failure mode, but they do have an impact on its final bearing capacity. The welding influence of upper and lower end plates affects columns with $\lambda \leq 85$, hence increasing weld spacing and size has no effect on the column's final bearing capacity. The column's ultimate bearing capacity increases significantly with $\lambda \geq 95$. The recommended spacing for intermittent welds in the project is 300mm-500mm, with a weld length of 30mm being the most cost-effective choice.

Funding

This work was supported by the National Natural Science Foundation of China [Grant No.52278150].

References

[1] H. Mashaly, A. H. A. Abdelrahman, F. A. Salem, N. S. Mahmoud. EVALUATION OF LOCAL-PLATE BUCKLING COEFFICIENT FOR THE DESIGN OF COLD-FORMED STEEL-LIPPED CHANNEL CROSS SECTIONS: NUMERICAL SIMULATIONS AND DESIGN RECOMMENDATIONS. Advanced Steel Construction. (2024): 20, 30-38.

[2] Affolter Ch., Piskoty G., Wullschleger L. Collapse of a high storage rack. Engineering Failure Analysis. (2009): 16: 1846-1855.

[3] Tian Y.S., Godley M.H.R., Wang J. Racking strength and stiffness of cold-formed steel wall frames. Journal of Constructional Steel Research. (2004), 7: 1069-1093.

[4] Gao, W, Wan, J & Liu, S 2021. A Stability Design Theory for the Steel Members Using Asymmetric Thin-Walled Open-Sections. Progress in Steel Building Structures. (2021) vol. 23, no. 5, pp. 53-62 and 72.

[5] Trouncer, Adam Nevil and Kim J.R. Rasmussen. Flexural–torsional buckling of ultra light-gauge steel storage rack uprights. Thin-walled Structures. 81 (2014): 159-174.

[6] Kilar, Vojko et al. Seismic analysis of an asymmetric fixed base and base-isolated high-rack steel structure. Engineering Structures. 33 (2011): 3471-3482.

[7] Obst, Maciej et al. Experimental investigation of four-point bending of thin walled open section steel beam loaded and set in the shear center. Scientific Reports. (2022): Vol:12, No.1:7275.

[8] Pala, Yaşar et al. Improvement of Buckling Behavior of Cold Formed Steel Uprights with Open Cross Section Used in Storage Rack Systems. World Academy of Science, Engineering and Technology, International Journal of Civil and Environmental Engineering. (2017): Vol:4, No:5.

[9] Davies, J. Michael et al. The design of perforated cold-formed steel sections subject to axial load and bending. Thin-walled Structures. 29 (1997): 141-157.

[10] Shanmugam, N. E. and M. Dhanalakshmi. Design for openings in cold-formed steel channel stub columns. Thin-walled Structures. 39 (2001): 961-981.

[11] Freitas, Arlene Maria Sarmanho et al. Analysis of steel storage rack columns. Journal of Constructional Steel Research. 61 (2005): 1135-1146.

[12] Moen, Cristopher Dennis and Benjamin W. Schafer. Elastic buckling of cold-formed steel columns and beams with holes. Engineering Structures. 31 (2009): 2812-2824.

[13] Baldassino, Nadia et al. An experimental investigation on solid and perforated steel storage racks uprights. Journal of Constructional Steel Research. (2019): Vol.155: 409-425.

[14] Talebian N, Gilbert B P, Pham C H, et al. Parametric Studies and Design Rules for Local and Distortional Biaxial-Bending Capacity of Cold-Formed Steel Storage-Rack Uprights. Journal of Structural Engineering. (2020): 146(3).

[15] Ren C, Wang B, Zhao X. Numerical predictions of distortional-global buckling interaction of perforated rack uprights in compression. Thin-Walled Structures. (2019): Vol.136:292-301.

[16] GB/T228.1-2021.Metallic materials—Tensile testing—Part 1: Method of test at room temperature.

[17] EN15512:2022. Steel static storage systems - Adjustable pallet racking systems - Principles for structural design.

[18] Zhao G. Study on stability performance of axial compression members of H-section of Q345GJ steel. Chongqing University. (2011).

[19] Qin Y. Theoretical and experimental study on axial compressive properties of cold-formed thin-walled steel low-rise residential wall column system. Tongji University. (2006).

[20] Shen Z, Guo X. Stability coefficient of compression rod of aluminum alloy extrusion profile with symmetrical cross-section. Journal of Building Structures. (2001): (04): 31-36+48.

[21] Casafont M, Roure F, Pastor M. Distortional buckling test for steel storage rack columns. Structures and Buildings. (2013): 166(8):392-402.

[22] Gu M, Zhang Q. Research on the introduction of first-order buckling modes as initial defects. Proceedings of the Fifth National Symposium on Modern Structural Engineering. (2005).

[23] GB50017-2017. Standard for design of steel structures.

[24] EN1993-1-5. Design of steel structures-Part1-5: Plated structural elements.

[25] Claudio Bernuzzi, Alice Pieri. Warping influence on the static design of unbraced steel storage pallet racks. Thin-Walled Structures. (2014), Vol.79:71-82.

[26] Claudio Bernuzzi, Castiglioni Carlo A. Experimental Analysis on the Cyclic Behavior of Beam-to-column Joints in Steel Storage Pallet Racks. Thin-Walled Structures. (2001): (39):841-859.

[27] J. J. Moy, C. S. Tan, EXPERIMENTAL STUDY OF SCISSOR FRAME STRUCTURES WITH FEM VALIDATION OF LOAD IMPACT ON MANUAL LOCKING MECHANISM. Advanced Steel Construction. (2024):20, 160-168.

[28] Aguirre C. Seismic Behavior of Rack Structures. Journal of Constructional Steel Research. (2005): 61(5): 607-624.

[29] Alavi B, Gupta A. Performance-Based Seismic Design of an Industrial Storage Rack System. Structures Congress. (2008):1-10.

[30] Aktepe, Rafet and Burcu Guldur Erkal. State-of-the-art review on measurement techniques and numerical modeling of geometric imperfections in cold-formed steel members. Journal of Constructional Steel Research. (2023): Vol.207:107942.